biosensors

MDPI

*Article*

# Bright NIR-Emitting Styryl Pyridinium Dyes with Large Stokes' Shift for Sensing Applications

**Nirasha I. Wickramasinghe [1,†], Brian Corbin [2,†], Devni Y. Kanakarathna [1,†], Yi Pang [2], Chathura S. Abeywickrama [2,*,‡] and Kaveesha J. Wijesinghe [1,*]**

[1] Department of Chemistry, Faculty of Science, University of Colombo, Colombo 00300, Sri Lanka
[2] Department of Chemistry, The University of Akron, Akron, OH 44325, USA
* Correspondence: cabeywic@outlook.com or cabeywic@stjude.org (C.S.A.); kwijesin@chem.cmb.ac.lk (K.J.W.)
† These authors contributed equally to this work.
‡ Present address: St Jude Children's Research Hospital, Memphis, TN 38105, USA.

**Abstract:** Two NIR-emitting donor-π-acceptor (D-π-A) type regioisomeric styryl pyridinium dyes (**1a**–**1b**) were synthesized and studied for their photophysical performance and environment sensitivity. The two regioisomers, **1a** and **1b**, exhibited interesting photophysical properties including, longer wavelength excitation ($\lambda_{ex} \approx 530$–$560$ nm), bright near-infrared emission ($\lambda_{em} \approx 690$–$720$ nm), high-fluorescence quantum yields ($\phi_{fl} \approx 0.24$–$0.72$) large Stokes' shift ($\Delta\lambda \approx 150$–$240$ nm) and high-environmental sensitivity. Probe's photophysical properties were studied in different environmental conditions such as polarity, viscosity, temperature, and concentration. Probes (**1a**–**1b**) exhibited noticeable changes in absorbance, emission and Stokes' shift while responding to the changes in physical environment. Probe **1b** exhibited a significant bathochromic shift in optical spectra ($\Delta\lambda \approx 20$–$40$ nm) compared to its isomer **1a**, due to the regio-effect. Probes (**1a**–**1b**) exhibited an excellent ability to visualize bacteria (*Bacillus megaterium*, *Escherichia coli*), and yeast (*Saccharomyces cerevisiae*) via fluorescence microscopy.

**Keywords:** styryl dyes; pyridinium; regio-effect; near-infrared dyes; fluorescence microscopy; donor-π-acceptor dyes; intramolecular charge transfer (ICT); Stokes' shift



**Citation:** Wickramasinghe, N.I.; Corbin, B.; Kanakarathna, D.Y.; Pang, Y.; Abeywickrama, C.S.; Wijesinghe, K.J. Bright NIR-Emitting Styryl Pyridinium Dyes with Large Stokes' Shift for Sensing Applications. *Biosensors* **2023**, *13*, 799. https://doi.org/10.3390/bios13080799

Received: 9 July 2023
Revised: 2 August 2023
Accepted: 7 August 2023
Published: 9 August 2023



## 1. Introduction

Styryl pyridinium dyes are an important class of conjugated small-molecules for developing efficient fluorescent imaging probes, laser dyes and photosensitizers [1–7]. The incorporation of the positively charged pyridinium moiety in to the conjugated π-system confers unique photophysical properties to these probes [8]. Donor-π-acceptor (D-π-A) molecules with advantageous photophysical properties can be formed by connecting a moderate to strong electron donating group (i.e., -OR -$NR_2$) into the conjugated π-system [9–12]. Such styryl pyridinium dyes (D-π-A) exhibit large Stokes' shift, high-fluorescence-quantum yields, improved photostability, high biocompatibility, enhanced solubility, and longer wavelength spectral profiles (i.e., far-red to near-infrared regions) [9,13–15]. Styryl pyridinium probes have been successfully exploited for several unique fluorescence imaging applications, including plasma membrane staining, mitochondria imaging and membrane potential determination, neuromast imaging in tissues and nucleus/DNA visualization [7,11,14,16–21]. The chemical stability, structural simplicity and bright longer-wavelength emission profiles of these probes are highly advantageous during fluorescence microscopy imaging. By incorporating a strong donor group (-$NR_2$) in to the probe architecture, interesting D-π-A type pyridinium probes were developed with a strong intramolecular charge transfer (ICT) ability, which produce large Stokes' shifts (i.e., $\Delta\lambda \approx 50$–$200$ nm) (Scheme 1) [9]. Such improved Stokes' shift can be highly beneficial for fluorescence microscopy imaging, as they can significantly reduce background interferences, improve penetration depth and mitigate self-quenching artifacts [9,22]. In

addition, ICT-based D-π-A type systems exhibit distinguishable optical responses (i.e., shift in emission/absorption maxima, increase/decrease in fluorescence intensity, ON/OFF in fluorescence, etc.) towards environmental changes that makes them ideal fluorescent sensing molecules [23–27]. Incorporating this principle in to action, several ratiometric, intensiometric and hybrid sensing probes were developed [23–27].

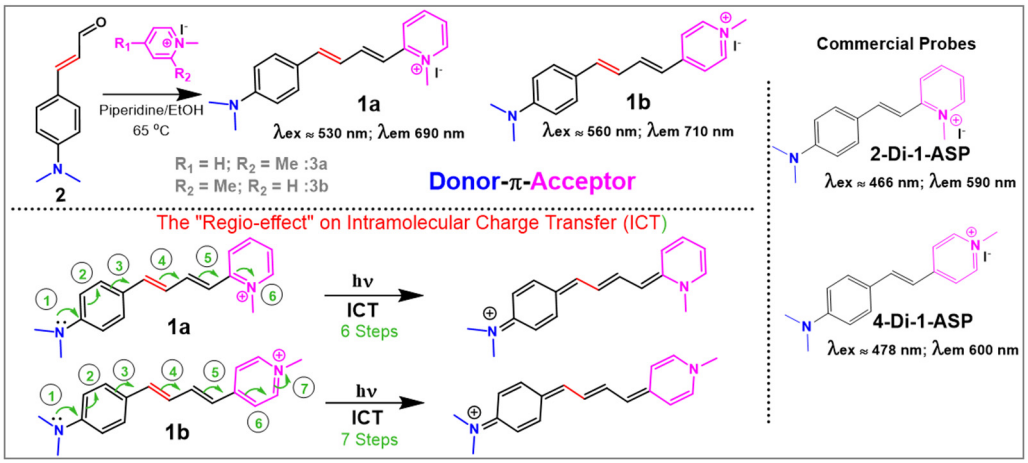


**Scheme 1.** Synthesis of probes **1a**-**1b** and ICT in probe **1a**.

2-Di-1-ASP and 4-Di-1-ASP (Scheme 1) are widely used and commercially available red-emitting ($\lambda_{ex}$ ≈ 466–475 nm; $\lambda_{em}$ ≈ 580–605 nm) D-π-A type pyridinium dyes that have several important applications in fluorescence microscopy imaging, including mitochondria visualization and membrane potential determination, plasma membrane staining, DNA staining and neuromast imaging in eukaryotic tissues (Scheme 1) [4,28,29]. In order to achieve high tissue penetrability and high biocompatibility, it is desirable to develop far-red to near-infrared (NIR) emitting dyes with longer excitation wavelength profiles and higher photostability [9,30–34]. One possible way to achieve NIR emission by extending conjugation length of the π-spacer group in D-π-A type architecture [9,35]. Inspired by this strategy, analogues with extended conjugation to 2-Di-1-ASP and 4-Di-1-ASP (i.e., **1a** and **1b** in Scheme 1) were reported with NIR-emission profiles ($\lambda_{ex}$ ≈ 530–560 nm; $\lambda_{em}$ ≈ 690–720 nm) [36–38]. Followed by previous reports [36–38], we have continued the study of photophysical performance and biosensing applications of probes **1a**–**1b** in this work. The key features of styryl pyridinium dyes **1a** and **1b** include: (1) bright NIR emission ($\phi_{fl}$ ≈ 0.24–0.72; $\lambda_{em}$ ≈ 690–720 nm), (2) high-environmental sensitivity and (3) mega Stokes' shift (i.e., Δλ ≈ 150–240 nm). In addition, probes **1a**–**1b** were excellent candidates to visualize microorganisms, such as *Bacillus megaterium*, *Escherichia coli*, and *Saccharomyces cerevisiae*, via widefield fluorescence microscopy. Probe **1** was also found to be an efficient fluorescent sensing candidate for quantifying albumin in aqueous environments with higher accuracy and lower detection limits.

## 2. Materials and Methods

All chemicals for synthesis were purchased from Acros Organics and VWR and used as they were received without further purification. Molecular biology grade reagents for bacterial cell culture and fluorescence microscopy imaging experiments were purchased from Thermo Fisher, Waltham, USA). NMR characterization data were acquired by Varian 500 MHz NMR spectrometer in deuterated DMSO-*d6*. High-resolution mass spectrometry (HRMS) data were acquired by an ESI-TOF MS system (Waters, Milford, MA, USA). UV-Vis studies were carried out in GENESYS 10S (Thermo Scientific, Waltham, MA, USA) and a Hewlett Packard-8453 (Agilent Technologies, Santa Clara, CA, USA) diode array spectrophotometers at 25 °C. Fluorescence spectroscopy studies were performed in HITACHI F7000 fluorescence spectrophotometer and a HORIBA Fluoromax-4 spectrofluorometer. Fluorescence lifetimes of the dyes were measured by using a time-correlated single-photon

counting (TCSPC) method on a Horiba DeltaPro lifetime system, which measures the lifetime range of 30 ps–1 s. This instrument is equipped with a picosecond photon detection module comprising a fast, cooled, photomultiplier with 230–850 nm response. All measurements were performed by exciting the sample solutions with a Horiba DeltaDiode™ DD-485 Laser (peak wavelength at 485 nm +/− 10 nm). Fluorescence microscopy imaging was performed in an Olympus BX53 inverted microscopy system with 100× and 40× magnification. Probes **1a**–**1b** were synthesized according to the previously reported procedure with modifications as reported in the methodology section [7,39].

### *2.1. General Procedure for Synthesis*

In a 10 mL round-bottom flask, 0.5 mmol of the 4-(Dimethylamino)cinnamaldehyde (**2**) was dissolved by adding 5 mL of anhydrous ethanol at room temperature with continuous stirring. To this bright orange solution, the corresponding methyl pyridinium salt (**3**) (0.5 mmol) was added followed by the addition of piperidine (0.5 mmol) with continuous stirring. The resulting dark-red solution was heated up with continuous stirring at 65 °C for 6 h. Upon completion of the reaction (checked by TLC), the dark-red colored reaction mixture was cooled down to room temperature and poured in to a 100 mL flask pre-filled with ethyl acetate (20 mL) while stirring continuously. The resulting dark red colored precipitate was collected by vacuum filtration and further washed with ethyl acetate (2 × 20 mL) and dried under the vacuum. The product was further purified with 5% methanol in dichloromethane by flash chromatography and dried under high vacuum.

*2-((1E,3E)-4-(4-(dimethylamino)phenyl)buta-1,3-dien-1-yl)-1-methylpyridin-1-ium iodide* (**1a**): Obtained as a bright red solid with 80% isolated yield. $^{1}$H NMR (500 MHz, DMSO-*d6*) δ 8.78 (dd, J = 6.4, 1.4 Hz, 1H), 8.40 (dd, J = 8.6, 1.6 Hz, 1H), 8.38–8.32 (m, 1H), 7.82 (dd, J = 15.0, 9.7 Hz, 1H), 7.74 (ddd, J = 7.6, 6.3, 1.6 Hz, 1H), 7.51–7.44 (m, 2H), 7.19–7.00 (m, 2H), 6.96 (d, J = 14.9 Hz, 1H), 6.78–6.72 (m, 2H), 4.23 (s, 3H), 3.00 (s, 6H). $^{13}$C NMR (126 MHz, DMSO-*d6*) δ 152.98, 151.72, 145.97, 145.56, 143.74, 143.26, 129.64, 124.14, 123.96, 123.77, 123.49, 117.23, 112.55, 56.49, 46.02. HRMS (TOF MS ES$^{+}$) found (*m*/*z*) for [M$^{+}$] 265.1706 [$C_{18}H_{21}N_2^{+}$]. HRMS calculated found (*m*/*z*) for [M$^{+}$] 265.1699 [$C_{18}H_{21}N_2^{+}$].

*4-((1E,3E)-4-(4-(dimethylamino)phenyl)buta-1,3-dien-1-yl)-1-methylpyridin-1-ium iodide* (**1b**): Obtained as a dark red solid with 75% isolated yield. $^{1}$H NMR (500 MHz, DMSO-*d6*) δ 8.63 (d, J = 6.5 Hz, 2H), 7.96 (d, J = 6.4 Hz, 2H), 7.73 (dt, J = 15.3, 5.0 Hz, 1H), 7.40 (d, J = 8.5 Hz, 2H), 6.94 (d, J = 5.1 Hz, 2H), 6.69–6.63 (m, 3H), 4.12 (s, 3H), 2.92 (s, 6H). $^{13}$C NMR (126 MHz, DMSO-*d6*) δ 153.21, 151.59, 144.97, 143.73, 142.49, 129.56, 124.00, 123.73, 123.54, 122.88, 112.50, 56.49, 46.96. HRMS (TOF MS ES$^{+}$) found (*m*/*z*) for [M$^{+}$] 265.1696 [$C_{18}H_{21}N_2^{+}$]. HRMS calculated found (*m*/*z*) for [M$^{+}$] 265.1699 [$C_{18}H_{21}N_2^{+}$].

### *2.2. Fluorescence Quantum Yields Calculation and Photophysical Property Evaluation*

Stock solutions of the probes (**1a**–**1b**) were prepared in spectroscopic grade DMSO at 10 mM concentration. For all spectroscopic studies (absorbance and emission), the working concentration of the probe was 1 × $10^{-5}$ M unless otherwise specified. While acquiring the emission spectra in different solvents, probes **1a** and **1b** were excited at 530 nm and the emissions were collected from 550 nm to 800 nm (unless otherwise specified). All spectroscopic studies were conducted in spectroscopic grade or double-distilled organic solvents. As all the fluorometric analysis data were acquired in diluted solutions (≈1 × $10^{-5}$ M or less), the collected spectra were not corrected for the inner filter-effects, assuming it is negligible [40–42].

The relative fluorescence quantum yields ($\phi_{fl}$) for probes (**1a**–**1b**) were calculated by using Rhodamine 6G as the standard (in ethanol), where the fluorescence quantum yield of Rhodamine 6G is 0.95 in ethanol. The following equation was used for the fluorescence quantum yield determination at 530 nm [43,44]**.**

$$(\phi_{fl})_{sample} = \phi_{ref} \times (A_{ref}/A_{sample}) \times [(I_{sample})/(I_{ref})] \times (\eta_{sample})^2/(\eta_{ref})^2$$

where $A$ is the absorbance of the sample, $I$ is the integrated fluorescence intensity and $\eta$ is the refractive index of the solvent.

### *2.3. Fluorescence Microscopy Imaging*

Two bacterial species (*Bacillus megaterium* and *Escherichia coli*) and a unicellular fungal species, *Saccharomyces cerevisiae*, were freshly cultured for fluorescence microscopy imaging experiments. Microorganisms were stained with 5 μM, 10 μM and 20 μM probe concentrations formed by diluting 1 μL of the stock solutions (made in DMSO) of the probes in aqueous media. *Bacillus megaterium* (Gram-positive) and *Escherichia coli* (Gram-negative) were grown in Luria broth (LB) agar plates. A sterilized loop was used to inoculate a single colony of bacteria from a streak plate into microcentrifuge tubes containing the appropriate concentration of the probe **1a** or **1b** in sterile water and incubated for 30 min at room temperature. After staining, a 4 μL culture volume was spotted on a glass slide and secured using a cover slip and the stained bacteria was then imaged by using a fluorescence microscope under 40× and 100× (oil) magnification. Images were acquired by exciting the stained specimen with 532 nm laser line with the standard Cy3 filter settings (580–620 nm) for the emission collection. *Saccharomyces cerevisiae* was grown in sterilized 250 mL conical flask by introducing 0.5 g of the baker's yeast in to a 100 mL sterile water for 2 h at 37 °C in a rotary shaker. Form this initial culture, 20 μL volume was transferred into a sterile eppendroff tube and staining solution (probe **1a** or **1b**) was introduced to make a final staining concentration of 5 μM, 10 μM or 20 μM. The resulting yeast suspensions were incubated for 30 min at room temperature. Followed by the incubation, 10 μL from each sample was mounted on glass slide, secured with cover slip and imaged by the fluorescence microscope under 40× and 100× magnification. Images were acquired by exciting stained specimens with 532 nm laser line with standard Cy3 filter settings (580–620 nm) for the emission collection. The bright-field images were acquired for all staining experiments.

## 3. Results

### *3.1. Optical Properties*

Optical properties (absorbance, emission, fluorescence quantum yield, molar absorptivity and Stokes' shift) of probes **1a** and **1b** were studied in different solvents and summarized in Table 1 and Figure 1. In summary, probes **1a** and **1b** exhibited excellent fluorescence quantum yields ($\phi_{fl} \approx 0.24$–$0.72$) and remarkably large Stokes' shifts $\Delta\lambda \approx 150$–$240$ nm (Table 1). The absorbance and emission spectra of **1a** ($\lambda_{abs} \approx 530$ nm; $\lambda_{em} \approx 690$ nm) and **1b** ($\lambda_{abs} \approx 560$ nm; $\lambda_{em} \approx 720$ nm) exhibit a noticeable bathochromic shift (i.e., red-shift) in comparison to their predecessors 2-Di-1-ASP($\lambda_{abs} \approx 465$ nm; $\lambda_{em} \approx 590$ nm) and 4-Di-1-ASP($\lambda_{abs} \approx 475$ nm; $\lambda_{em} \approx 605$ nm), respectively (Scheme 1). This large bathochromic shift, observed in the optical spectra of **1** ($\Delta\lambda_{abs} \approx 80$ nm; $\Delta\lambda_{em} \approx 100$ nm), is attributed to the extension of the π-spacer conjugation length (in between the donor-acceptor assembly) by adding an extra double bond (Scheme 1) [45]. Similar to 2-Di-1-ASP and 4-Di-1-ASP dyes, **1a** and **1b** also exhibited a similar trend in the shift in their optical spectra due to the "regio-effect" (see Scheme 1 and Figure 1). The para-methyl pyridinium linkage (i.e., **1b** and 4-Di-1-ASP) exhibited a noticeable bathochromic shift in their optical spectra ($\Delta\lambda_{abs} \approx 10$–$20$ nm; $\Delta\lambda_{em} \approx 20$–$40$ nm), compared to the regio-isomeric ortho-methyl pyridinium linkage (i.e., **1a** and 2-Di-1-ASP), as a result of the extended donor-accepter interactions across the π-system via an additional resonance step (i.e., longer conjugation), as shown in the Scheme 1 (i.e., regio-effect). Probe **1** also exhibited higher fluorescence quantum yields ($\phi_{fl} \approx 0.24$–$0.72$) compared to the predecessors with shorter conjugation length (i.e., 2-Di-1-ASP and 4-Di-1-ASP) (Table 1). These results imply that the strength of the ICT interaction and length of the conjugated system play important roles towards the quantum efficiency of the fluorophores [46–48]. Both **1a** and **1b** were highly sensitive towards the nature of the solvent (i.e., polarity), thus changing solvent polarity from non-polar to polar showed a noticeable shift in the spectral position (Figure 1 and Table 1). In weakly polar solvents such as DCM or $CHCl_3$, probe **1** exhibited a large bathochromic shift

in the absorbance ($\lambda_{abs} \approx$ 540–560 nm) compared to polar protic solvents such as water or methanol ($\lambda_{abs} \approx$ 440–490 nm) (Figure 1). The observed negative solvatochromism (i.e., hypsochromic effect) in the absorption profile can be justified by considering the solvation-induced extra stabilization of the polar ground-state (i.e., HOMO level) compared to the less polar first-excited state of the probe **1** by polar protic solvents (i.e., water, ethanol or methanol) [49,50]. As a consequence, the energy gap in between HOMO-LUMO will rise, thus a noticeable hypsochromic shift (i.e., blue-shift) will occur in the absorption spectra [49,50]. Due to the positively charged nature of probe **1**, it is certain that polar solvents can significantly stabilize the probe's ground-state than a non-polar or weakly polar solvent (i.e., ion-dipole interactions) [45]. Although it is not as prominent as in the absorption spectra, a careful observation will emphasize the solvatochromic nature of the emission properties of the probes (Figure 1 and Table 1). In weakly polar solvents (i.e., $CHCl_3$), probe **1** exhibited an emission at $\lambda_{em} \approx$ 667–688 nm and in polar aprotic solvents, such as DMSO, a noticeable red-shift (i.e., bathochromic effect) was observed at $\lambda_{em} \approx$ 698–730 nm in the emission (Table 1 and Figure 1). As a result of the strong solvation interaction in polar solvent environments, a positive solvatochromic effect was thus observed for the probe's emission spectra by lowering the energy of the emissive ICT state (i.e., strong ICT) [45,51]. Therefore, this strong optical response towards solvent polarity can be exploited as a sensing mechanism to develop robust environmentally sensitive fluorescent dyes. It is also important to note that moving from organic (i.e., DCM) to aqueous (i.e., water) environments leads to a significant decrease in the fluorescence quantum yields of the probes, which suggests their potential as "wash-free" stains for fluorescence microscopy imaging [7,11,52]. The observed significant quenching in fluorescence was reported as a solvent-assisted non-radiative pathway (i.e., quenching mechanism) that was studied extensively for solvatochromic organic fluorophores [53,54]. This observed low fluorescence quantum yield in aqueous environments is a well-known characteristic of many wash-free staining D-π-A type fluorescent imaging dyes [9].

**Table 1.** Spectroscopic properties of probes **1a** and **1b**.

| Solvent | DCM | $CHCl_3$ | ACN | DMSO | DMF | EtOH | MeOH | Water |
|---|---|---|---|---|---|---|---|---|
| **Probe 1a** | | | | | | | | |
| $\lambda_{abs}$ (nm) | 541 | 512 | 478 | 477 | 476 | 488 | 482 | 438 |
| $\lambda_{em}$ (nm) | 678 | 667 | 687 | 698 | 694 | 684 | 688 | 687 |
| Δλ (nm) | 137 | 155 | 209 | 221 | 218 | 196 | 206 | 249 |
| $\phi_{fl}$ | 0.61 | 0.29 | 0.33 | 0.68 | 0.40 | 0.24 | 0.38 | 0.01 |
| ε ($M^{-1}\cdot cm^{-1}$) | 47,023 | 42,456 | 41,482 | 41,470 | 40,700 | 42,428 | 39,647 | 33,162 |
| **Probe 1b** | | | | | | | | |
| $\lambda_{abs}$ (nm) | 561 | 530 | 487 | 489 | 490 | 501 | 492 | 446 |
| $\lambda_{em}$ (nm) | 706 | 688 | 718 | 731 | 724 | 714 | 712 | 718 |
| Δλ (nm) | 145 | 158 | 231 | 242 | 234 | 213 | 220 | 272 |
| $\phi_{fl}$ | 0.72 | 0.47 | 0.24 | 0.61 | 0.48 | 0.38 | 0.31 | 0.005 |
| ε ($M^{-1}\cdot cm^{-1}$) | 48,120 | 43,442 | 43,100 | 49,406 | 42,100 | 42,159 | 40,477 | 25,670 |

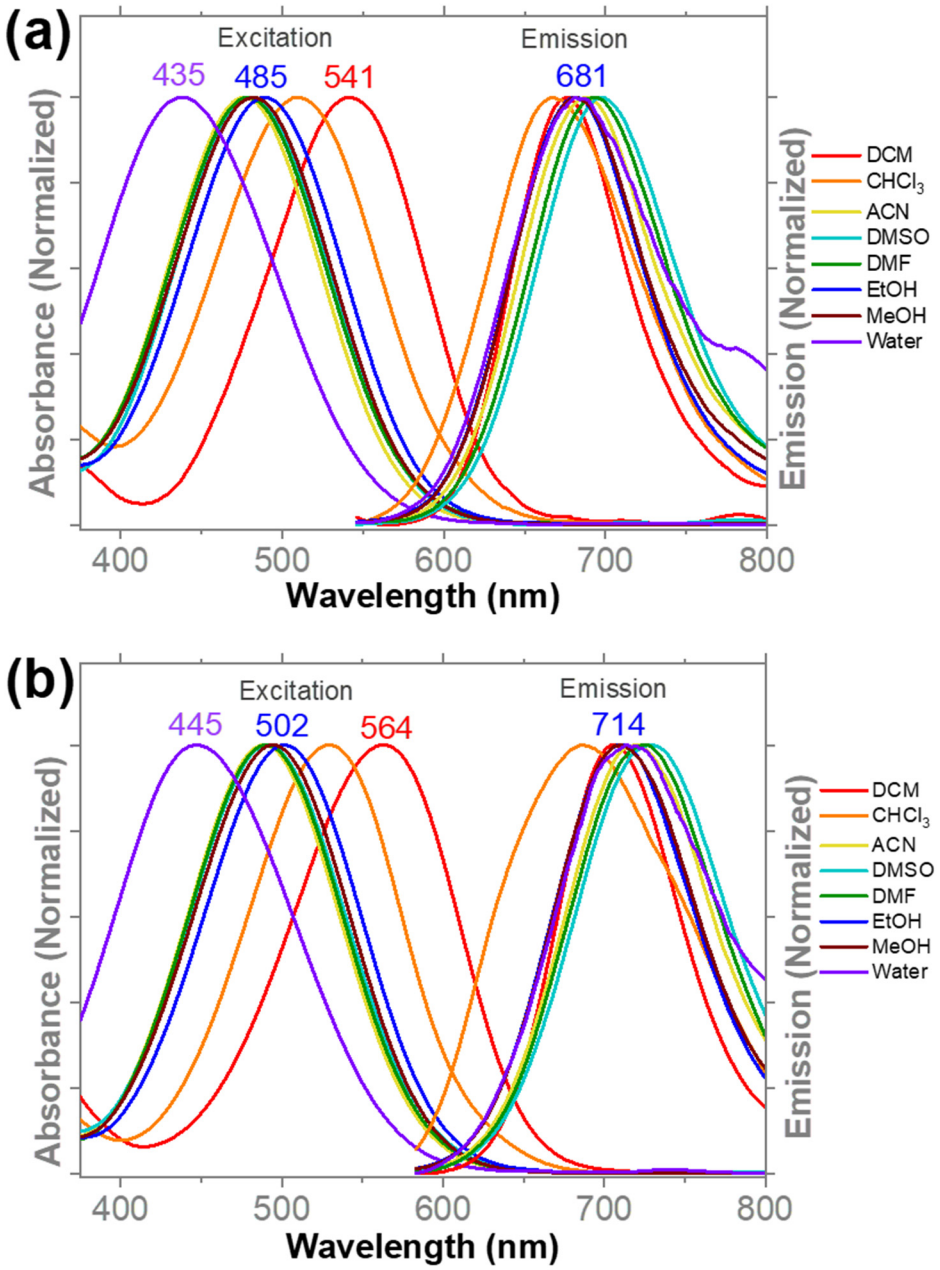


**Figure 1.** Normalized absorbance and emission spectra acquired for probe **1a** (**a**) and **1b** (**b**) in different solvents. Optical spectra were recorded for probes at $1 \times 10^{-6}$ M and 25 °C. For the emission collection, probe **1a** was excited at 500 nm and **1b** was excited at 520 nm. Emission spectra were collected from 540 nm to 800 nm range.

To investigate the impact of the concentration towards optical properties, absorption and emission spectra were acquired at different probe concentrations from 10 μM to 50 μM (Figure S2). The absorption spectra of both **1a** and **1b** exhibited a linear regression, indicating no noticeable impact on the probe's solubility within the tested concentration range (Figure S2). However, the emission spectra of both probes exhibited a moderate decrease in the increment, resulting in a non-linear regression at higher probe concentrations (i.e., 40 μM or higher). Since the absorbance spectra do not show this pattern, one can easily rule out the possibility of aggregation at higher concentrations. Therefore, this unusual trend in the emission intensities is likely to occur due to the inner filter effect at higher probe concentrations (Figure S2). As expected, probes exhibited a noticeable intensiometric response towards changes in viscosity of the solvent environment in a methanol:glycerol

mixture exhibiting an excellent environmental sensitivity (Figure S3). Increasing solvent viscosity led to a significant improvement in the emission signals of **1a** and **1b**, where no changes in the absorption spectra were observed (Figure S3). Therefore, based on the experimental outcomes, these styryl pyridinium D-π-A systems will be very useful in developing viscosity-sensing NIR fluorescent dyes [55–58].

### *3.2. Sensing Human Serum Albumin (HSA) by Fluorometry*

Fluorescence quantum yields calculated for the probes exhibited a significant decrease while moving from organic (non-polar) solvents to aqueous (polar) solvents (Table 1). With this observation, we hypothesized that probe **1** will produce a large intensiometric response in emission if successfully internalized in to a hydrophobic environment from the aqueous solution. To test this hypothesis, we have introduced human serum albumin (HSA), a well-known water-soluble small molecule binding transporter protein in to the aqueous environment [39,59,60]. Spectrometric titrations were performed for probes **1a** and **1b** in the aqueous solutions with 5% HSA in room-temperature (Figure 2). As we hypothesized, probe **1a** and **1b** exhibited a significant fluorescence enhancement (by 7 fold and 24 fold, respectively) upon addition of HSA, indicating possible internalization in to the hydrophobic binding pockets in HSA of the protein (Figure 2) [39,61]. It is important to note that probe **1b** exhibited a higher sensitivity (i.e., 3 times than **1a**) towards HSA than **1a** based on experimental findings (Figure 2). This high sensitivity observed for **1b** indicates distinct advantages of its structural geometry (see Scheme 1) towards efficient binding interactions (i.e., hydrophobic interactions) [39].

The limit of detection (LOD) and limit of quantification (LOQ) values were calculated for both probes by extracting linearly fitted regions of the probe's response curves via regression analysis. The calculated LOD values for probes **1a** and **1b** were 0.059 mg/mL and 0.043 mg/mL, respectively (Table S1). During the spectrometric titrations, the absorption spectra of the probes did not exhibit any noticeable changes, which is indicative of no structural changes or covalent interactions taking place upon binding events (Figure S4). Besides this large intensiometric response in fluorescence signal, a highly noticeable blue-shift (i.e., hypsochromic effect) in the emission profiles was also observed for **1a** ($\lambda_{em} \approx$ 685 nm to 650 nm) and **1b** ($\lambda_{em} \approx$ 715 nm to 662 nm) during the spectrometric titrations (Figure 2). This large hypsochromic effect is indicative of possible geometric stabilization of the probe in hydrophobic protein environments to enhance binding interactions, which was discussed during previous work [39,62,63]. The probe-albumin binding events were validated by measuring intrinsic fluorescence quenching of HSA at $\lambda_{em} \approx 346$ due to relocation of the protein towards more hydrophobic environments via hydrophobic probe-protein interactions (ESI Figure S4) [64–67]. In addition, the solution stability of probe-albumin complexes were analyzed in aqueous solution by recording optical spectra (absorbance and emission) of the probe–protein complex as a function of time (Figure S5). Probe **1a** and **1b**'s albumin complexes exhibited stable fluorescence signals over 2 h, indicating an excellent stability in the solution (Figure S5). Therefore, the architecture of probe **1** will be highly useful in developing potential albumin sensing fluorescent dyes that can be used in aqueous biological environments. Since **1a** and **1b** are positively charged, they were tested against various anionic species (~10 equivalence) in solution to determine any possible interactions (i.e., electrostatic). Based on the optical spectra analysis, the probes did not exhibit any noticeable response towards any of the anionic species tested (Figure S6).

### *3.3. Low-Temperature and Fluorescence Lifetime Studies*

In order to understand the significance of ICT and the impact of the regio-effect in two isomeric probe designs (i.e., **1a** and **1b**), we acquired low temperature fluorescence spectra for the probes in ethanol (Figure 3). Ethanolic solutions of **1a** and **1b** were frozen to −180 °C in a liquid nitrogen dewer instantly to limit molecular rotations and bond reorganizations that are associated with the subsequent ICT process. At ultra-low temperatures (i.e., −180 °C), **1a** and **1b** exhibited their emissions at $\lambda_{em} \approx$ 578 nm and $\lambda_{em} \approx$ 590 nm,

respectively (Figure 3a,b) The significant blue-shift observed in the emission spectra suggested that, at a frozen matrix (i.e., −189 °C), the ICT process is hindered due to restricted molecular rotation. Thus, a large hypsochromic shift in the emission spectra ($\Delta\lambda \approx 82$ nm for **1a** and $\Delta\lambda \approx 108$ nm for **1b**) was observed. Most importantly, the acquired excitation spectra did not change at low-temperature conditions (i.e., −180 °C), suggesting no structural changes associated with the frozen matrix conditions (Figure 3a,b). These data clearly indicate that the observed NIR emission in probe **1** solely depends on the efficiency of the ICT process. The fluorescence lifetime measurement of **1a** revealed a two-exponential decay pattern with $\tau1 = 0.20$ ns (95.8%) and $\tau2 = 0.80$ ns (4.2%) with the best curve fitting of reduce chi-square, $\chi^2_r = 1.12$ (Figure 3c) in acetonitrile. Similarly, **1b** exhibited a two-exponential decay with $\tau1 = 0.23$ ns (91.7%) and $\tau2 = 0.43$ ns (8.3%) with the best curve fitting of reduce chi-square, $\chi^2_r = 0.96$ (Figure 3d). The two observed exponential decay patterns with two lifetime components can be attributed to the two excited states (i.e., LE and ICT), as reported in previous findings for similar probes [68].

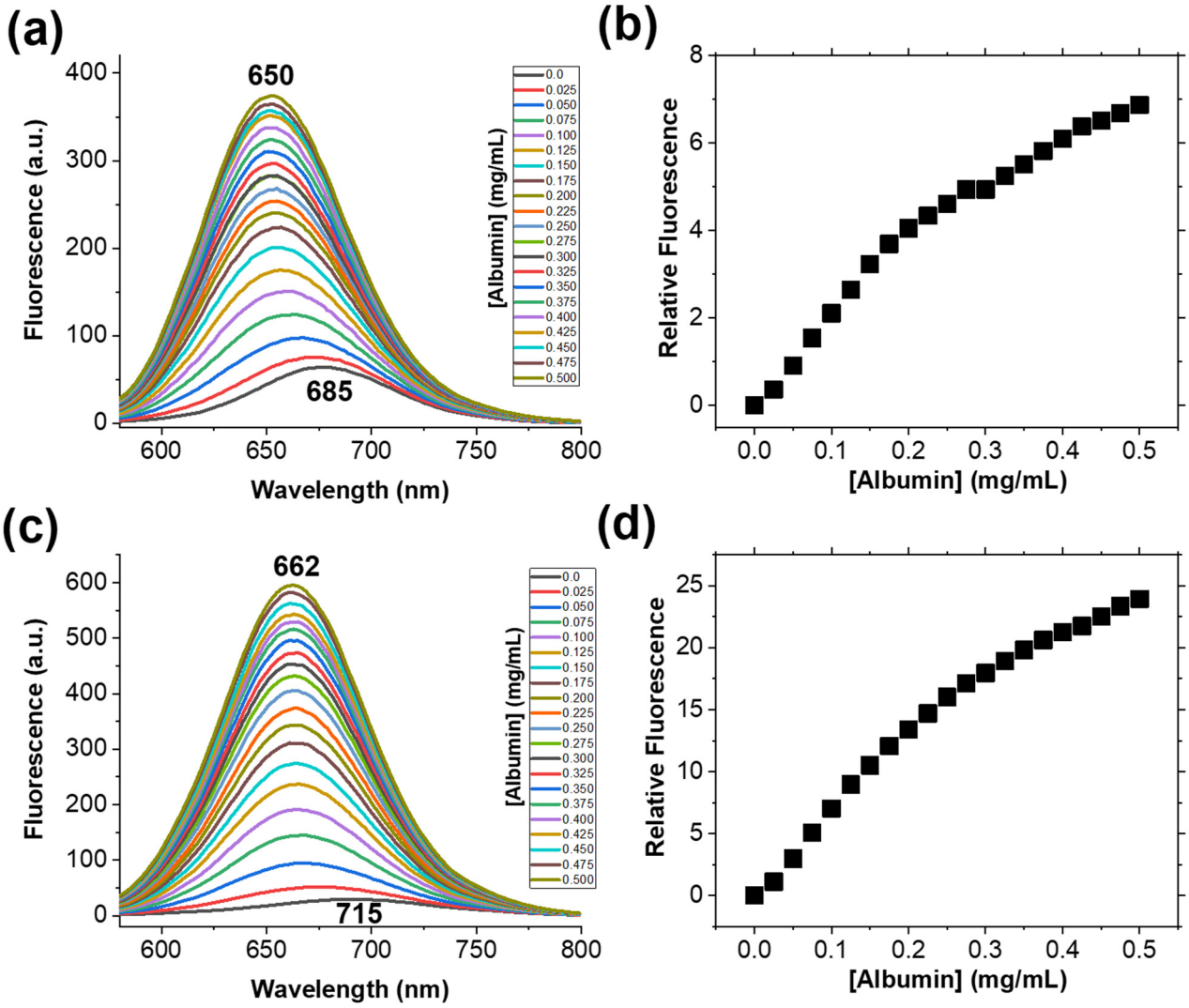


**Figure 2.** The fluorescence emission spectra acquired during the spectrometric titrations of probes **1a** (**a**) and **1b** (**c**) at $1 \times 10^{-6}$ M concentration with a 5% HSA solution in water at room temperature. Figures (**b**) and (**d**) represents the relative fluorescence signal recorded at the emission maxima as a function of HSA concentration in the solution for probes **1a** and **1b**, respectively. Probes were excited at 520 nm and the emission spectra were collected from 540 nm to 800 nm range.

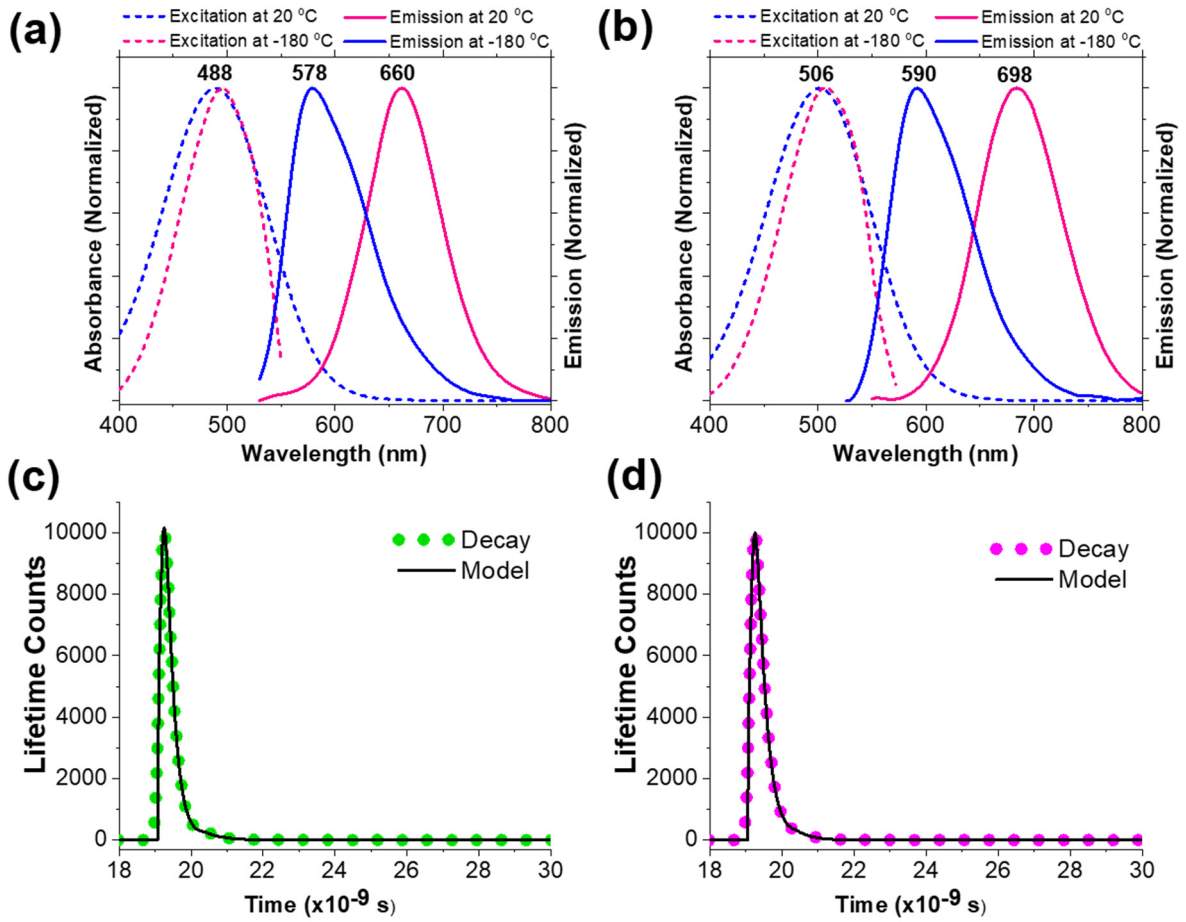


**Figure 3.** The low-temperature excitation and emission analysis for probes **1a** ($1 \times 10^{-6}$ M; (**a**)) and **1b** ($1 \times 10^{-6}$ M; (**b**)) in absolute ethanol. **1a** and **1b** were excited at 485 nm and 505 nm, respectively. (**c**,**d**) represents data obtained by using the time-correlated single-photon counting (TCSPC) method for lifetime measurements. Sample: solutions of dye **1a** (**c**) and **1b** (**d**) in acetonitrile (under Ar). Excitation: 485 nm Lasers. Data were collected by using a 650 nm long path filter. Reference: scattering solution. Result: $\tau 1 = 0.20$ ns, $\tau 2 = 0.80$ ns; $\chi^2 = 1.12$ for **1a** and $\tau 1 = 0.23$ ns, $\tau 2 = 0.44$ ns; $\chi^2 = 0.96$ for **1b**.

### *3.4. Visualizing Microorganisms via Fluorescence Microscopy*

Some recent research have highlighted the potential of styryl pyridinium dyes as excellent fluorescent bacterial stains (i.e., *Escherichia coli*) for fluorescent microscopy applications [14,69]. Also, several commercially available fluorescent bacterial stains, such as FM-1-43, consist of styryl pyridinium moiety in the structure [4]. Therefore, we hypothesized that probe **1a** and **1b** will be ideal candidates for staining bacteria for fluorescence microscopy imaging. Since probe **1** exhibited outstanding photophysical properties (i.e., bright NIR emission, high fluorescence quantum yield, longer wavelength excitation and large Stokes' shift) that are suitable for a potential imaging candidate, we decided to perform fluorescence microscopy imaging experiments with different microorganisms (*Bacillus megaterium*, *Escherichia coli*, and *Saccharomyces cerevisiae*) [9]. Thus, two bacterial cultures, *Bacillus megaterium* (Gram-positive) and *Escherichia coli* (Gram-negative), were grown in appropriate growth media and stained with varying concentrations of probe **1a** and **1b** (5 μM, 10 μM and 20 μM), as explained in the methodology. Interestingly, both *Bacillus megaterium* and *Escherichia coli* cells stained with probe **1a** and **1b** exhibited bright emission patterns indicating the probe's potential to visualize both Gram-positive and Gram-negative bacterial strains (Figures 4 and 5) by fluorescence microscopy. The uniform bright-red emission patterns arising from the stained bacterial cells indicated that the probes are likely visualizing

the plasma membranes of the strains, as reported in previous findings [14,69]. Also, it is important to note that probes (**1a** and **1b**) did not produce background interference/noise during fluorescence microscopy imaging experiments. This characteristic of the probe can be attributed to the significant fluorescent quantum yield (or brightness) difference observed from organic (i.e., DCM) vs. aqueous (i.e., water) environments, which will likely facilitate bright fluorescence emission upon internalization into hydrophobic cellular environments of the microorganisms such as the plasma membrane (Table 1). Therefore, these probes (**1a** and **1b**) will be ideal candidates for wash-free fluorescence imaging applications where the post-staining washing step is impossible to perform without perturbation to the specimen. Previously reported work showed that small-molecule cationic probes, such as **1**, may likely interact with the surface of the microorganism via electrostatic and/or hydrophobic interactions [70,71]. Therefore, it is certain that the positively charged nature of the probe plays a key role towards observed specificity [70–73]. In order to further evaluate the potential of these probes to visualize other microorganisms, we decided to stain yeast cells (*Saccharomyces cerevisiae*) with 10 μM concentration of the probe (**1a** or **1b**) for fluorescence microscopy imaging (Figures 4 and 5). Interestingly, yeast cells stained with probe **1** exhibited uniform bright-red fluorescence patterns similar to what was observed for bacterial species, thus indicating possible internalization in to the cells (Figures 4 and 5). The observed bright red fluorescence also suggested that probes may likely accumulate in to the hydrophobic cores within the cells (i.e., plasma membrane and/or organelle membranes) and not in to the aqueous cytoplasm. However, unfortunately, no further studies were possible due to the limited availability of the imaging infrastructure.

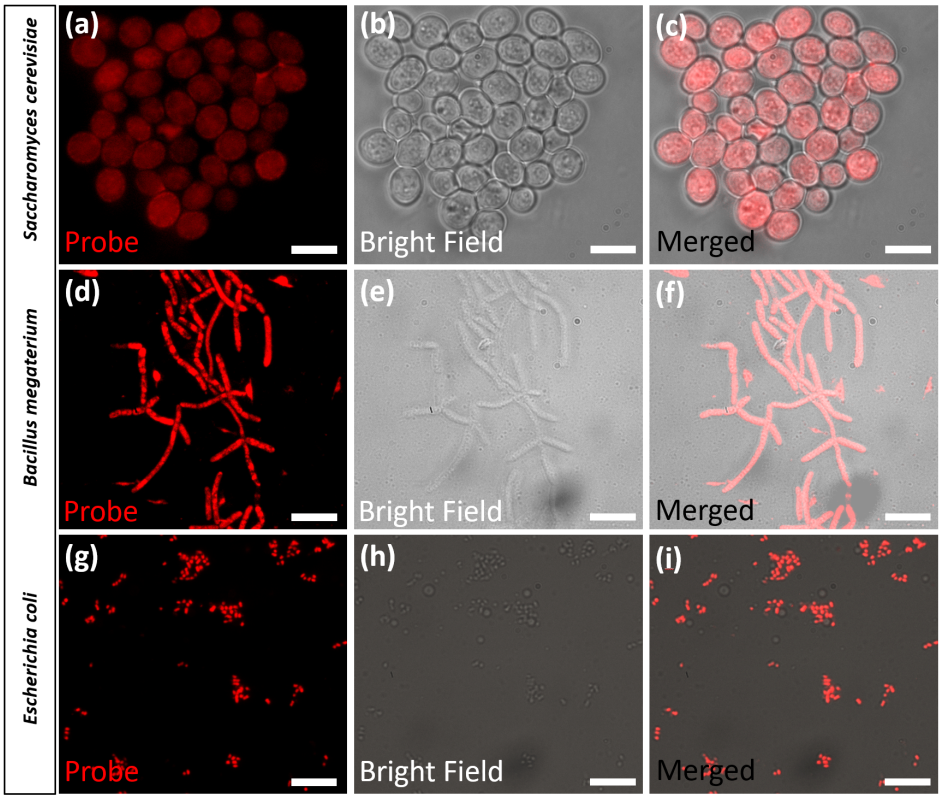


**Figure 4.** Fluorescence microscopy images obtained from *Saccharomyces cerevisiae* (**a**–**c**), *Bacillus megaterium* (**d**–**f**), and *Escherichia coli* (**g**–**i**), stained with probe **1a** (10 μM) for 30 min. Images (**a**–**i**) represents, probe **1a** emission in the cells (**a**,**d**,**g**), bright field images (**b**,**e**,**h**), and merged images (**c**,**f**,**i**). Images were acquired by exciting the stained organisms with 532 nm laser line with standard Cy3 filter settings (580–620 nm) for the emission collection. The scale bar indicates a 20-micron region.

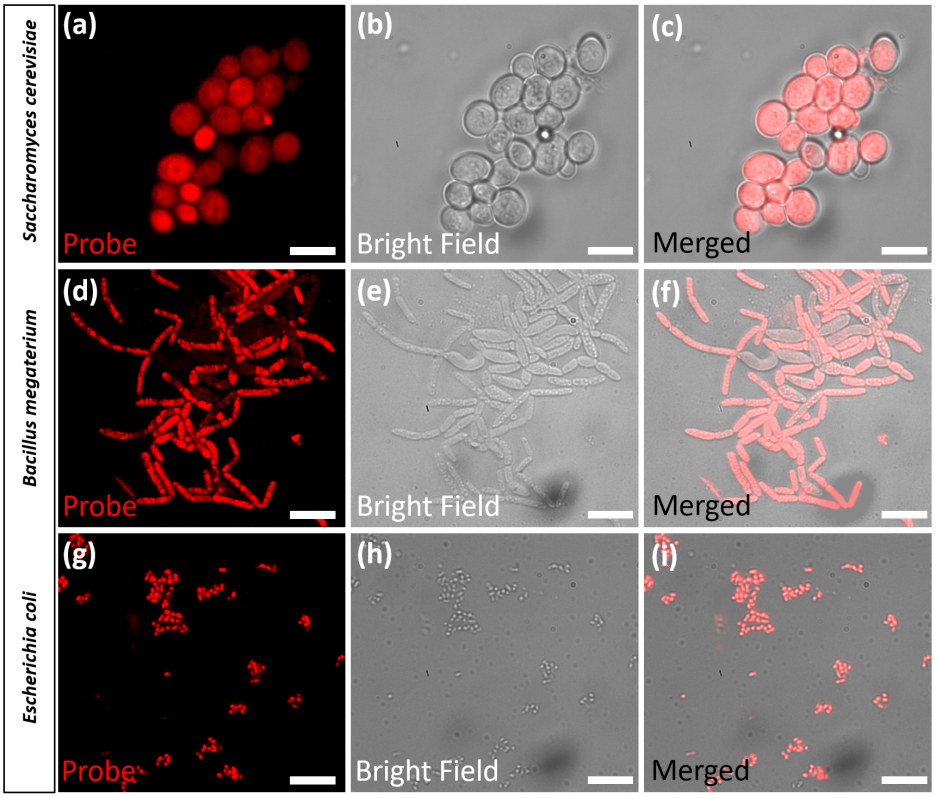


**Figure 5.** Fluorescence microscopy images obtained from *Saccharomyces cerevisiae* (**a**–**c**), *Bacillus megaterium* (**d**–**f**), and *Escherichia coli* (**g**–**i**), stained with probe **1b** (10 μM) for 30 min. Images (**a**–**i**) represents, probe **1b** emission in the cells (**a**,**d**,**g**), bright field images (**b**,**e**,**h**), and merged images (**c**,**f**,**i**). Images were acquired by exciting the stained organism with 532 nm laser line with standard Cy3 filter settings (580–620 nm) for the emission collection. The scale bar indicates a 20-micron region.

## 4. Conclusions

In summary, two styryl-pyridinium containing fluorescent imaging dyes (**1a**–**1b**) were developed by utilizing donor-π-acceptor (D-π-A) architecture in the presence of strong donor groups (-$NMe_2$). Due to the presence of a strong electron donating group (i.e., -$NMe_2$), probes exhibited strong intramolecular charge transfer (ICT) activity, which evolved to very large Stokes' shifts ($\Delta\lambda > 150$ nm). Probes exhibited bright near-infrared fluorescence ($\lambda_{em} \approx 690$–$730$ nm; $\phi_{fl} \approx 0.24$–$0.72$) and high-environment sensitivity (i.e., solvent polarity, viscosity, and temperature). Probe **1b** exhibited a noticeable bathochromic shift in optical spectra when compared to its regio-isomer **1a** due to the regio-effect, which enables extended ICT interaction across the conjugated system via resonance. The impact of the ICT process was studied by low-temperature fluorescence analysis. Probes (**1a** and **1b**) exhibited an excellent ability to quantify human serum albumin in aqueous solutions by fluorometry with calculated LOD values at 0.059 mg/mL (**1a**) and 0.043 mg/mL (**1b**), respectively. The NIR emission, extremely large fluorescence quantum yield difference in organic vs aqueous environments and longer wavelength excitation profile, suggested that probes **1a** and **1b** are ideal fluorescent staining agents for bioimaging applications. Probes exhibited exceptional potential to visualize Gram-positive and Gram-negative bacteria (i.e., *Bacillus megaterium*, *Escherichia coli*) and yeast (i.e., *Saccharomyces cerevisiae*) by fluorescence microscopy with no background interference. Based on these highly desirable and unique photophysical properties with its microorganism staining ability, probe **1** will provide powerful molecular designs in the near future to develop robust fluorescent imaging dyes.

**Supplementary Materials:** The following supporting information can be downloaded at: https://www.mdpi.com/article/10.3390/bios13080799/s1, Figure S1: Characterization data; Figure S2: Concentration dependency of the optical properties; Figure S3: Viscosity dependency of the optical properties; Figure S4: Spectrometric titration of the probes with HSA; Figure S5: Stability evaluation for the probe-albumin complex; Figure S6: Sensitivity of the probes towards anions and other species; Figure S7: Solid-state emission spectra analysis; Table S1: Limit of detection (LOD) and limit of quantification (LOQ) calculation.

**Author Contributions:** Conceptualization, K.J.W., C.S.A. and Y.P.; methodology, C.S.A. and K.J.W.; validation, C.S.A., K.J.W. and Y.P.; formal analysis, N.I.W., B.C. and D.Y.K.; resources, K.J.W. and Y.P.; data curation, N.I.W., B.C. and D.Y.K.; writing—original draft preparation, C.S.A., N.I.W. and K.J.W.; writing—review and editing, C.S.A. and K.J.W.; supervision, K.J.W., C.S.A. and Y.P. All authors have read and agreed to the published version of the manuscript.

**Funding:** This research received no external funding.

**Institutional Review Board Statement:** Not Applicable.

**Informed Consent Statement:** Not applicable.

**Data Availability Statement:** Not applicable.

**Acknowledgments:** Authors Acknowledge Sujatha Hewage, C.D. Wijayarathna and M.D.P de Costa from The Department of Chemistry, University of Colombo, Sri Lanka.

**Conflicts of Interest:** The authors declare no conflict of interest.

## References

1. Deligeorgiev, T.; Vasilev, A.; Kaloyanova, S.; Vaquero, J.J. Styryl Dyes–Synthesis and Applications during the Last 15 Years. *Color. Technol.* **2010**, *126*, 55–80. [CrossRef]
2. Zhao, C.F.; Gvishi, R.; Narang, U.; Ruland, G.; Prasad, P.N. Structures, Spectra, and Lasing Properties of New (Aminostyryl) Pyridinium Laser Dyes. *J. Phys. Chem.* **1996**, *100*, 4526–4532. [CrossRef]
3. Li, T.-Y.; Su, C.; Akula, S.B.; Sun, W.-G.; Chien, H.-M.; Li, W.-R. New Pyridinium Ylide Dyes for Dye Sensitized Solar Cell Applications. *Org. Lett.* **2016**, *18*, 3386–3389. [CrossRef] [PubMed]
4. Johnson, I.; Spence, M.T.Z. *The Handbook: A Guide to Fluorescent Probes and Labeling Technologies*; Molecular Probes Inc.: Eugene, OR, USA, 2010.
5. Shindy, H.A. Fundamentals in the Chemistry of Cyanine Dyes: A Review. *Dyes Pigment.* **2017**, *145*, 505–513. [CrossRef]
6. Bohländer, P.R.; Wagenknecht, H.-A. Synthesis and Evaluation of Cyanine–Styryl Dyes with Enhanced Photostability for Fluorescent DNA Staining. *Org. Biomol. Chem.* **2013**, *11*, 7458–7462. [CrossRef]
7. Abeywickrama, C.S.; Wijesinghe, K.J.; Plescia, C.B.; Fisher, L.S.; Goodson, T., III; Stahelin, R.V.; Pang, Y. A Pyrene-Based Two-Photon Excitable Fluorescent Probe to Visualize Nuclei in Live Cells. *Photochem. Photobiol. Sci.* **2020**, *19*, 1152–1159. [CrossRef]
8. Abeywickrama, C.S.; Pang, Y. Synthesis of a Bis [2-(2′-Hydroxyphenyl) Benzoxazole] Pyridinium Derivative: The Fluoride-Induced Large Spectral Shift for Ratiometric Response. *New J. Chem.* **2021**, *45*, 9102–9108. [CrossRef]
9. Abeywickrama, C.S. Large Stokes Shift Benzothiazolium Cyanine Dyes with Improved Intramolecular Charge Transfer (ICT) for Cell Imaging Applications. *Chem. Commun.* **2022**, *58*, 9855–9869. [CrossRef]
10. Ayadi, A.; Szukalski, A.; El-Ghayoury, A.; Haupa, K.; Zouari, N.; Myśliwiec, J.; Kajzar, F.; Kulyk, B.; Sahraoui, B. TTF Based Donor-Pi-Acceptor Dyads Synthesized for NLO Applications. *Dyes Pigment.* **2017**, *138*, 255–266. [CrossRef]
11. Abeywickrama, C.S.; Wijesinghe, K.J.; Stahelin, R.V.; Pang, Y. Bright Red-Emitting Highly Reliable Styryl Probe with Large Stokes Shift for Visualizing Mitochondria in Live Cells under Wash-Free Conditions. *Sens. Actuators B Chem.* **2019**, *285*, 76–83. [CrossRef]
12. Abeywickrama, C.S.; Bertman, K.A.; Pang, Y. From Nucleus to Mitochondria to Lysosome Selectivity Switching in a Cyanine Probe: The Phenolic to Methoxy Substituent Conversion Affects Probe's Selectivity. *Bioorg. Chem.* **2020**, *99*, 103848. [CrossRef]
13. Kurtaliev, E.N. Spectroscopic Study of Interaction of Styrylcyanine Dye Sbt and Its Derivatives with Bovine Serum Albumin. *J. Lumin.* **2012**, *132*, 2281–2287. [CrossRef]
14. Dahal, D.; Ojha, K.R.; Alexander, N.; Konopka, M.; Pang, Y. An NIR-Emitting ESIPT Dye with Large Stokes Shift for Plasma Membrane of Prokaryotic (*E. coli*) Cells. *Sens. Actuators B Chem.* **2018**, *259*, 44–49. [CrossRef]
15. Yashchuk, V.M.; Gusak, V.V.; Dmytruk, I.M.; Prokopets, V.M.; Kudrya, V.Y.; Losytskyy, M.Y.; Tokar, V.P.; Gumenyuk, Y.O.; Yarmoluk, S.M.; Kovalska, V.B. Two-Photon Excited Luminescent Styryl Dyes as Probes for the DNA Detection and Imaging. Photostability and Phototoxic Influence on DNA. *Mol. Cryst. Liq. Cryst.* **2007**, *467*, 325–338. [CrossRef]
16. Bhadani, A.; Singh, S. Novel Gemini Pyridinium Surfactants: Synthesis and Study of Their Surface Activity, DNA Binding, and Cytotoxicity. *Langmuir* **2009**, *25*, 11703–11712. [CrossRef] [PubMed]

17. Banerjee, S.; Kitchen, J.A.; Gunnlaugsson, T.; Kelly, J.M. The Effect of the 4-Amino Functionality on the Photophysical and DNA Binding Properties of Alkyl-Pyridinium Derived 1, 8-Naphthalimides. *Org. Biomol. Chem.* **2013**, *11*, 5642–5655. [CrossRef] [PubMed]
18. Zhang, Y.; Wang, L.; Rao, Q.; Bu, Y.; Xu, T.; Zhu, X.; Zhang, J.; Tian, Y.; Zhou, H. Tuning the Hydrophobicity of Pyridinium-Based Probes to Realize the Mitochondria-Targeted Photodynamic Therapy and Mitophagy Tracking. *Sens. Actuators B Chem.* **2020**, *321*, 128460. [CrossRef]
19. Reedy, J.L.; Hedlund, D.K.; Gabr, M.T.; Henning, G.M.; Pigge, F.C.; Schultz, M.K. Synthesis and Evaluation of Tetraarylethylene-Based Mono-, Bis-, and Tris (Pyridinium) Derivatives for Image-Guided Mitochondria-Specific Targeting and Cytotoxicity of Metastatic Melanoma Cells. *Bioconjug. Chem.* **2016**, *27*, 2424–2430. [CrossRef] [PubMed]
20. Loew, L.M.; Cohen, L.B.; Dix, J.; Fluhler, E.N.; Montana, V.; Salama, G.; Jian-young, W. A Naphthyl Analog of the Aminostyryl Pyridinium Class of Potentiometric Membrane Dyes Shows Consistent Sensitivity in a Variety of Tissue, Cell, and Model Membrane Preparations. *J. Membr. Biol.* **1992**, *130*, 1–10. [CrossRef]
21. Ermakova, Y.G.; Sen, T.; Bogdanova, Y.A.; Smirnov, A.Y.; Baleeva, N.S.; Krylov, A.I.; Baranov, M.S. Pyridinium Analogues of Green Fluorescent Protein Chromophore: Fluorogenic Dyes with Large Solvent-Dependent Stokes Shift. *J. Phys. Chem. Lett.* **2018**, *9*, 1958–1963. [CrossRef]
22. Li, Y.; Dahal, D.; Abeywickrama, C.S.; Pang, Y. Progress in Tuning Emission of the Excited-State Intramolecular Proton Transfer (ESIPT)-Based Fluorescent Probes. *ACS Omega* **2021**, *6*, 6547–6553. [CrossRef]
23. Xu, Y.; Liu, Y.; Qian, X. Novel Cyanine Dyes as Fluorescent PH Sensors: PET, ICT Mechanism or Resonance Effect? *J. Photochem. Photobiol. A Chem.* **2007**, *190*, 1–8. [CrossRef]
24. Coto, P.B.; Serrano-Andrés, L.; Gustavsson, T.; Fujiwara, T.; Lim, E.C. Intramolecular Charge Transfer and Dual Fluorescence of 4-(Dimethylamino)Benzonitrile: Ultrafast Branching Followed by a Two-Fold Decay Mechanism. *Phys. Chem. Chem. Phys.* **2011**, *13*, 15182. [CrossRef]
25. Song, S.; Ju, D.; Li, J.; Li, D.; Wei, Y.; Dong, C.; Lin, P.; Shuang, S. Synthesis and Spectral Characteristics of Two Novel Intramolecular Charge Transfer Fluorescent Dyes. *Talanta* **2009**, *77*, 1707–1714. [CrossRef] [PubMed]
26. Sasaki, S.; Drummen, G.P.C.; Konishi, G. Recent Advances in Twisted Intramolecular Charge Transfer (TICT) Fluorescence and Related Phenomena in Materials Chemistry. *J. Mater. Chem. C* **2016**, *4*, 2731–2743. [CrossRef]
27. Suzuki, Y.; Yokoyama, K. Design and Synthesis of Intramolecular Charge Transfer-Based Fluorescent Reagents for the Highly-Sensitive Detection of Proteins. *J. Am. Chem. Soc.* **2005**, *127*, 17799–17802. [CrossRef]
28. Keij, J.F.; Bell-Prince, C.; Steinkamp, J.A. Staining of Mitochondrial Membranes with 10-nonyl Acridine Orange MitoFluor Green, and MitoTracker Green Is Affected by Mitochondrial Membrane Potential Altering Drugs. *Cytom. J. Int. Soc. Anal. Cytol.* **2000**, *39*, 203–210. [CrossRef]
29. Rytting, E.; Bryan, J.; Southard, M.; Audus, K.L. Low-Affinity Uptake of the Fluorescent Organic Cation 4-(4-(Dimethylamino) Styryl)-N-Methylpyridinium Iodide (4-Di-1-ASP) in BeWo Cells. *Biochem. Pharmacol.* **2007**, *73*, 891–900. [CrossRef]
30. Luo, S.; Zhang, E.; Su, Y.; Cheng, T.; Shi, C. A Review of NIR Dyes in Cancer Targeting and Imaging. *Biomaterials* **2011**, *32*, 7127–7138. [CrossRef]
31. Escobedo, J.O.; Rusin, O.; Lim, S.; Strongin, R.M. NIR Dyes for Bioimaging Applications. *Curr. Opin. Chem. Biol.* **2010**, *14*, 64–70. [CrossRef]
32. Daehne, S.; Resch-Genger, U.; Wolfbeis, O.S. *Near-Infrared Dyes for High Technology Applications*; Springer Science & Business Media: Berlin/Heidelberg, Germany, 2012; Volume 52, ISBN 9401151024.
33. Samanta, A.; Vendrell, M.; Das, R.; Chang, Y.-T. Development of Photostable Near-Infrared Cyanine Dyes. *Chem. Commun.* **2010**, *46*, 7406–7408. [CrossRef]
34. Swamy, P.C.A.; Sivaraman, G.; Priyanka, R.N.; Raja, S.O.; Ponnuvel, K.; Shanmugpriya, J.; Gulyani, A. Near Infrared (NIR) Absorbing Dyes as Promising Photosensitizer for Photo Dynamic Therapy. *Coord. Chem. Rev.* **2020**, *411*, 213233. [CrossRef]
35. Abeywickrama, C.S.; Baumann, H.J.; Alexander, N.; Shriver, L.P.; Konopka, M.; Pang, Y. NIR-Emitting Benzothiazolium Cyanines with an Enhanced Stokes Shift for Mitochondria Imaging in Live Cells. *Org. Biomol. Chem.* **2018**, *16*, 3382–3388. [CrossRef]
36. Carlotti, B.; Benassi, E.; Barone, V.; Consiglio, G.; Elisei, F.; Mazzoli, A.; Spalletti, A. Effect of the π Bridge and Acceptor on Intramolecular Charge Transfer in Push–Pull Cationic Chromophores: An Ultrafast Spectroscopic and TD-DFT Computational Study. *ChemPhysChem* **2015**, *16*, 1440–1450. [CrossRef]
37. Agnihotri, H.; Vasu, A.K.; Palakollu, V.; Kanvah, S. Neutral and Cationic Pyridylbutadienes: Solvatochromism and Fluorescence Response with Sodium Cholate. *Photochem. Photobiol. Sci.* **2015**, *14*, 2159–2167. [CrossRef]
38. Li, C.; Plamont, M.-A.; Aujard, I.; Le Saux, T.; Jullien, L.; Gautier, A. Design and Characterization of Red Fluorogenic Push–Pull Chromophores Holding Great Potential for Bioimaging and Biosensing. *Org. Biomol. Chem.* **2016**, *14*, 9253–9261. [CrossRef]
39. Abeywickrama, C.S.; Li, Y.; Ramanah, A.; Owitipana, D.N.; Wijesinghe, K.J.; Pang, Y. Albumin-Induced Large Fluorescence Turn ON in 4-(Diphenylamino)Benzothiazolium Dyes for Clinical Applications in Protein Detection. *Sens. Actuators B Chem.* **2022**, *368*, 132199. [CrossRef]
40. Panigrahi, S.K.; Mishra, A.K. Inner Filter Effect in Fluorescence Spectroscopy: As a Problem and as a Solution. *J. Photochem. Photobiol. C Photochem. Rev.* **2019**, *41*, 100318.
41. Chen, S.; Yu, Y.-L.; Wang, J.-H. Inner Filter Effect-Based Fluorescent Sensing Systems: A Review. *Anal. Chim. Acta* **2018**, *999*, 13–26. [CrossRef]

42. Wang, T.; Zeng, L.-H.; Li, D.-L. A Review on the Methods for Correcting the Fluorescence Inner-Filter Effect of Fluorescence Spectrum. *Appl. Spectrosc. Rev.* **2017**, *52*, 883–908. [CrossRef]
43. Williams, A.T.R.; Winfield, S.A.; Miller, J.N. Relative Fluorescence Quantum Yields Using a Computer-Controlled Luminescence Spectrometer. *Analyst* **1983**, *108*, 1067–1071. [CrossRef]
44. Langhals, H.; Karolin, J.; Johansson, L.B.-Å. Spectroscopic Properties of New and Convenient Standards for Measuring Fluorescence Quantum Yields. *J. Chem. Soc. Faraday Trans.* **1998**, *94*, 2919–2922.
45. Bertman, K.A.; Abeywickrama, C.S.; Pang, Y. A NIR Emitting Cyanine with Large Stokes' Shift for Mitochondria and Identification of Their Membrane Potential Disruption. *ChemBioChem* **2022**, *23*, e202100516. [CrossRef] [PubMed]
46. Yamaguchi, Y.; Matsubara, Y.; Ochi, T.; Wakamiya, T.; Yoshida, Z. How the π Conjugation Length Affects the Fluorescence Emission Efficiency. *J. Am. Chem. Soc.* **2008**, *130*, 13867–13869. [CrossRef]
47. Duncan, T.V.; Susumu, K.; Sinks, L.E.; Therien, M.J. Exceptional Near-Infrared Fluorescence Quantum Yields and Excited-State Absorptivity of Highly Conjugated Porphyrin Arrays. *J. Am. Chem. Soc.* **2006**, *128*, 9000–9001. [CrossRef] [PubMed]
48. Zhang, Z.; Zhang, G.; Wang, J.; Sun, S.; Zhang, Z. The Mechanisms of Large Stokes Shift and Fluorescence Quantum Yields in Anilino Substituted Rhodamine Analogue: TICT and PICT. *Comput. Theor. Chem.* **2016**, *1095*, 44–53.
49. Lu, H.; Rutan, S.C. Solvatochromic Studies on Reversed-Phase Liquid Chromatographic Phases. 2. Characterization of Stationary and Mobile Phases. *Anal. Chem.* **1996**, *68*, 1387–1393. [CrossRef]
50. Cha, S.; Choi, M.G.; Jeon, H.R.; Chang, S.-K. Negative Solvatochromism of Merocyanine Dyes: Application as Water Content Probes for Organic Solvents. *Sens. Actuators B Chem.* **2011**, *157*, 14–18.
51. Muraoka, H.; Obara, T.; Ogawa, S. Systematic Synthesis, Comparative Studies of the Optical Properties, and the ICT-Based Sensor Properties of a Series of 2, 4, 6-Tri (5-Aryl-2-Thienyl) Pyrimidines with the D–π–A System. *Tetrahedron Lett.* **2016**, *57*, 3011–3015. [CrossRef]
52. Abeywickrama, C.S.; Wijesinghe, K.J.; Stahelin, R.V.; Pang, Y. Lysosome Imaging in Cancer Cells by Pyrene-Benzothiazolium Dyes: An Alternative Imaging Approach for LAMP-1 Expression Based Visualization Methods to Avoid Background Interference. *Bioorg. Chem.* **2019**, *91*, 103144.
53. Maillard, J.; Klehs, K.; Rumble, C.; Vauthey, E.; Heilemann, M.; Fürstenberg, A. Universal Quenching of Common Fluorescent Probes by Water and Alcohols. *Chem. Sci.* **2021**, *12*, 1352–1362. [CrossRef] [PubMed]
54. Lee, S.F.; Vérolet, Q.; Fürstenberg, A. Improved Super-Resolution Microscopy with Oxazine Fluorophores in Heavy Water. *Angew. Chem. Int. Ed.* **2013**, *52*, 8948–8951. [CrossRef]
55. Cao, J.; Wu, T.; Hu, C.; Liu, T.; Sun, W.; Fan, J.; Peng, X. The Nature of the Different Environmental Sensitivity of Symmetrical and Unsymmetrical Cyanine Dyes: An Experimental and Theoretical Study. *Phys. Chem. Chem. Phys.* **2012**, *14*, 13702–13708.
56. Er, J.C.; Tang, M.K.; Chia, C.G.; Liew, H.; Vendrell, M.; Chang, Y.-T. MegaStokes BODIPY-Triazoles as Environmentally Sensitive Turn-on Fluorescent Dyes. *Chem. Sci.* **2013**, *4*, 2168–2176. [CrossRef]
57. Wagner, B.D. The Use of Coumarins as Environmentally-Sensitive Fluorescent Probes of Heterogeneous Inclusion Systems. *Molecules* **2009**, *14*, 210–237. [PubMed]
58. Wang, C.; Sato, Y.; Kudo, M.; Nishizawa, S.; Teramae, N. Ratiometric Fluorescent Signaling of Small Molecule, Environmentally Sensitive Dye Conjugates for Detecting Single-Base Mutations in DNA. *Chem. Eur. J.* **2012**, *18*, 9481–9484. [PubMed]
59. Kim, Y.; Shin, E.; Jung, W.; Kim, M.K.; Chong, Y. A Near-Infrared Turn-on Fluorescent Sensor for Sensitive and Specific Detection of Albumin from Urine Samples. *Sensors* **2020**, *20*, 1232. [CrossRef]
60. van der Vusse, G.J. Albumin as Fatty Acid Transporter. *Drug Metab. Pharmacokinet.* **2009**, *24*, 300–307. [CrossRef] [PubMed]
61. Ràfols, C.; Amézqueta, S.; Fuguet, E.; Bosch, E. Molecular Interactions between Warfarin and Human (HSA) or Bovine (BSA) Serum Albumin Evaluated by Isothermal Titration Calorimetry (ITC), Fluorescence Spectrometry (FS) and Frontal Analysis Capillary Electrophoresis (FA/CE). *J. Pharm. Biomed. Anal.* **2018**, *150*, 452–459.
62. Mallick, A.; Haldar, B.; Chattopadhyay, N. Spectroscopic Investigation on the Interaction of ICT Probe 3-Acetyl-4-Oxo-6,7-Dihydro-12H Indolo-[2,3-a] Quinolizine with Serum Albumins. *J. Phys. Chem. B* **2005**, *109*, 14683–14690. [CrossRef]
63. Li, Y.; He, W.; Dong, Y.; Sheng, F.; Hu, Z. Human Serum Albumin Interaction with Formononetin Studied Using Fluorescence Anisotropy, FT-IR Spectroscopy, and Molecular Modeling Methods. *Bioorg. Med. Chem.* **2006**, *14*, 1431–1436.
64. Chatterjee, S.; Mukherjee, T.K. Effect of Self-Association of Bovine Serum Albumin on the Stability of Surfactant-Induced Aggregates of Allylamine-Capped Silicon Quantum Dots. *J. Phys. Chem. B* **2013**, *117*, 16110–16116.
65. Yang, F.; Zhang, Y.; Liang, H. Interactive Association of Drugs Binding to Human Serum Albumin. *Int. J. Mol. Sci.* **2014**, *15*, 3580–3595. [CrossRef] [PubMed]
66. Epps, D.E.; Raub, T.J.; Caiolfa, V.; Chiari, A.; Zamai, M. Determination of the Affinity of Drugs toward Serum Albumin by Measurement of the Quenching of the Intrinsic Tryptophan Fluorescence of the Protein. *J. Pharm. Pharmacol.* **1999**, *51*, 41–48. [CrossRef]
67. Tayyab, S.; Izzudin, M.M.; Kabir, M.Z.; Feroz, S.R.; Tee, W.-V.; Mohamad, S.B.; Alias, Z. Binding of an Anticancer Drug, Axitinib to Human Serum Albumin: Fluorescence Quenching and Molecular Docking Study. *J. Photochem. Photobiol. B Biol.* **2016**, *162*, 386–394.
68. Ramadass, R.; Bereiter-Hahn, J. Photophysical Properties of DASPMI as Revealed by Spectrally Resolved Fluorescence Decays. *J. Phys. Chem. B* **2007**, *111*, 7681–7690. [PubMed]

69. Xiong, W.; Wang, L.; Chen, X.; Tang, H.; Cao, D.; Zhang, G.; Chen, W. Pyridinium-Substituted Tetraphenylethylene Salt-Based Photosensitizers by Varying Counter Anions: A Highly Efficient Photodynamic Therapy for Cancer Cell Ablation and Bacterial Inactivation. *J. Mater. Chem. B* **2020**, *8*, 5234–5244. [PubMed]
70. Yuan, H.; Liu, Z.; Liu, L.; Lv, F.; Wang, Y.; Wang, S. Cationic Conjugated Polymers for Discrimination of Microbial Pathogens. *Adv. Mater.* **2014**, *26*, 4333–4338. [CrossRef] [PubMed]
71. Li, Z.; Lu, W.; Jia, S.; Yuan, H.; Gao, L.-H. Design and Application of Conjugated Polymer Nanomaterials for Detection and Inactivation of Pathogenic Microbes. *ACS Appl. Bio Mater.* **2020**, *4*, 370–386. [CrossRef] [PubMed]
72. Liu, N.; Gujrati, V.; Werner, J.P.F.; Mishra, K.; Anzenhofer, P.; Stiel, A.C.; Mettenleiter, G.; Feuchtinger, A.; Walch, A.; Ntziachristos, V. Bacterial Outer Membrane Vesicles as Cationic Dye Carriers for Optoacoustics-Guided Phototherapy of Cancer. *Cancer Nanotechnol.* **2023**, *14*, 36. [CrossRef]
73. Budin, G.; Chung, H.J.; Lee, H.; Weissleder, R. A 'Magnetic'Gram Stain for Bacterial Detection. *Angew. Chem. Int. Ed. Engl.* **2012**, *51*, 7752. [CrossRef] [PubMed]